JACS Au
AN OPEN ACCESS JOURNAL OF THE AMERICAN CHEMICAL SOCIETY

pubs.acs.org/jacsau

Article

Resolving Halide Ion Stabilization through Kinetically Competitive Electron Transfers

Alexander M. Deetz and Gerald J. Meyer*

Cite This: *JACS Au* 2022, 2, 985−995

Read Online

ACCESS | Metrics & More | Article Recommendations | Supporting Information

ABSTRACT: Stabilization of ions and radicals often determines reaction kinetics and thermodynamics, but experimental determination of the stabilization magnitude remains difficult, especially when the species is short-lived. Herein, a competitive kinetic approach to quantify the stabilization of a halide ion toward oxidation imparted by specific stabilizing groups relative to a solvated halide ion is reported. This approach provides the increase in the formal reduction potential, $\Delta E^{\circ\prime}(X^{\bullet/-})$, where X = Br and I, that results from the noncovalent interaction with stabilizing groups. The $[Ir(dF\text{-}(CF_3)\text{-}ppy)_2(tmam)]^{3+}$ photocatalyst features a dicationic ligand tmam [4,4′-bis[(trimethylamino)methyl]-2,2′-bipyridine]$^{2+}$ that is shown by ^{1}H NMR spectroscopy to associate a single halide ion, $K_{eq} = 7 \times 10^4$ M^{-1} (Br^-) and $K_{eq} = 1 \times 10^4$ M^{-1} (I^-). Light excitation of the photocatalyst in halide-containing acetonitrile solutions results in competitive quenching by the stabilized halide and the more easily oxidized diffusing halide ion. Marcus theory is used to relate the rate constants to the electron-transfer driving forces for oxidation of the stabilized and unstabilized halide, the difference of which provides the increase in reduction potentials of $\Delta E^{\circ\prime}(Br^{\bullet/-}) = 150 \pm 24$ meV and $\Delta E^{\circ\prime}(I^{\bullet/-}) = 67 \pm 13$ meV. The data reveal that K_{eq} is a poor indicator of these reduction potential shifts. Furthermore, the historic and widely used assumption that Coulombic interactions alone are responsible for stabilization must be reconsidered, at least for polarizable halogens.

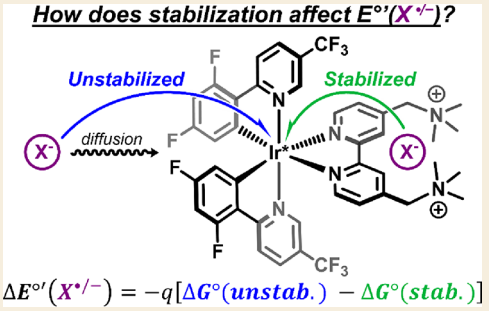

KEYWORDS: *halide oxidation, halide stabilization, excited states, bimolecular electron transfer, time-resolved spectroscopy, anion sensing, photoredox, photocatalysis, solar energy storage*

INTRODUCTION

Stabilization provided by local environments to redox-active ions such as halides, as well as their radical counterparts, is a critical factor that often determines the kinetics and thermodynamics of reactions in chemistry and biology. For example, dehalogenase enzymes contain cationic and/or H-bonding protein residues in the active site that provide a stabilizing interaction to the departing halide that is critical to C−X bond (X = Cl, Br, I) cleavage and catalytic activity.[1−7] Likewise, the reactivity and selectivity of enantioselective Pictet−Spengler- and Mannich-type reactions—where the interaction of a hydrogen-bonding catalyst with a halide−ion pair is responsible for asymmetric induction[8−11]—are highly dependent on the identity of the halide, suggesting that the strength of the halide's interaction is of paramount importance.[9] In solar energy conversion and storage applications, photocatalysts have been used to drive the thermodynamically uphill oxidation of halides to generate solar fuels.[12−15] To this end, halide-selective ion sequestration from complex mixtures is relevant to their selective oxidation with the ultimate goal of using ubiquitous halide sources, such as chloride in sea water. However, the sequestration chemistry is generally expected to stabilize the halide, rendering it more difficult to oxidize. We note that for halides, hydroxides, and other species unstable in adjacent oxidation states that are of tremendous interest to biologists and chemists alike, standard electrochemical techniques do not report on the one-electron oxidation and instead report on multielectron processes coupled with bond formation (for instance, $3I^- \rightarrow I_3^- + 2e^-$). Therefore, kinetic measurements provide the sole method to infer thermodynamic information on redox couples such as $E^{\circ\prime}(X^{\bullet/-})$.[16] This submission reports a comparative method to quantify the increase in the formal reduction potential, $E^{\circ\prime}(X^{\bullet/-})$, imparted to the halide by sequestration relative to a freely diffusing halide ion.

Recently reported H-bonding macrocycles[17] exhibit remarkable selectivity for Cl^- sequestration from aqueous solutions with sequestering affinities up to 10^{17} M^{-1}, akin to the crown ethers[18,19] and cryptands[20] developed for binding cations a generation earlier. However, it is known that halide sequestration with affinities of only 10^4 M^{-1} has led to such

Received: February 11, 2022
Revised: March 28, 2022
Accepted: March 29, 2022
Published: April 12, 2022

ACS Publications

© 2022 The Authors. Published by American Chemical Society

https://doi.org/10.1021/jacsau.2c00088
JACS Au 2022, 2, 985−995

significant halide stabilization that they were no longer oxidized by photocatalysts, while freely diffusing halides were still reactive.[21,22] This observation has been interpreted as a perturbation to $E^{\circ\prime}(X^{\bullet/-})$ afforded by sequestration that preferentially stabilizes the anionic form of the halogen species. Recent pulse radiolysis studies have shown that even "inert" electrolytes can stabilize redox-active ions by hundreds of millivolts.[23−25] These examples highlight the need to develop a stronger understanding of how noncovalent interactions affect the kinetics and thermodynamics of electron transfer, and more broadly, any reaction where ion stabilization impacts reactivity.

$$X^- + SG^{n+} \rightleftharpoons [X, SG]^{(n-1)+}$$

$$\Delta G^\circ_{eq} = -RT\ln(K_{eq}) \quad (1)$$

The Gibbs free energy change for the interaction of an ion, X^-, with a stabilizing group, SG^{n+}, is related to the association equilibrium constant, K_{eq}, shown in eq 1, which can be measured through numerous techniques. While a large K_{eq} implies significant charge transfer and an increase in $E^{\circ\prime}(X^{\bullet/-})$, the value reports on the halide anion stabilization but does not necessarily indicate the magnitude of the potential shift.

Consider, for example, the hypothetical scenario that is commonly invoked where the free energy change for the equilibrium is solely due to the Coulombic attraction of two charged moieties with no other intermolecular forces at play; ion-pair formation occurs with a free energy change, ΔG_{eq}° (Scheme 1a). If either the halide or the SG^+ species underwent redox chemistry that rendered its charge neutral such as oxidation of X^- to $X^\bullet$, then ΔG°_{eq} would approach zero in this hypothetical scenario. This implies that ΔG°_{eq} manifests directly as a perturbation of $E^{\circ\prime}(X^{\bullet/-})$ to $E^{\circ\prime}(SG^+,X^{\bullet/-})^{+/0}$. Indeed, ΔG°_{eq} has previously been used to estimate the perturbation to reduction potentials that result from ion pairing.[25] However, this scenario assumes that there are no stabilizing interactions for the electron-transfer products in the redox equilibrium. This assumption is rarely reasonable in chemistry and biology, yet is the sole contribution considered in time-honored photochemical analysis[26,27] and state-of-the-art kinetic measurements.[23,24,28] This assumption is particularly problematic in determination of $E^{\circ\prime}(SG^+, X^{\bullet/-})^{+/0}$ as the K_{eq} values do not account for noncovalent interactions with the halogen atom that would be particularly important for polarizable halide ions like iodide. Therefore, experimental methods to determine how ion stabilization through noncovalent interactions impacts formal reduction potentials are critically needed.

Scheme 1. (a) Thermochemical Cycle for Halide and Halogen Atom Stabilization by a Stabilizing Group, SG. (b) Generic Strategy for a Photocatalyst Functionalized with a SG that Impacts the Formal Reduction Potential of a Redox-Active Ion, X^-

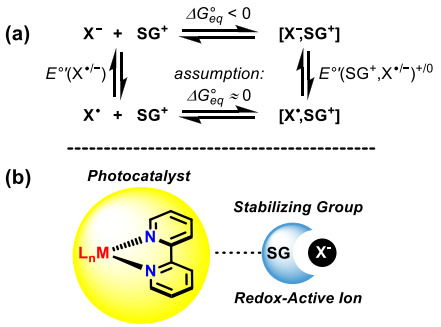

Here, we report a new experimental approach for measuring the change in reduction potential, $\Delta E^{\circ\prime}(X^{\bullet/-})$, of a stabilized halide ion relative to an unstabilized ion. The approach takes advantage of robust and easily derivatized photocatalysts and the relationship between kinetics and thermodynamics in semiclassical Marcus theory[29] as follows: (1) synthesize a photocatalyst modified with ion stabilizing group(s) that are weakly electronically coupled to the excited state (Scheme 1b); (2) quantify excited-state electron-transfer rate constants for the stabilized and unstabilized ions; and (3) utilize Marcus theory to determine the driving forces, $-\Delta G^\circ_{et}$, for both electron-transfer reactions. The difference in the Gibbs free energy change for the two reactions yields $\Delta E^{\circ\prime}(X^{\bullet/-})$ imparted by the stabilizing group(s), $\Delta E^{\circ\prime}(X^{\bullet/-}) = -q[\Delta G_{et}^\circ(\text{unstab.}) - G_{et}^\circ(\text{stab.})]$, where $q = 1$ for a $1e^-$ electron transfer. This strategy requires some assumptions inherent to Marcus theory, but a sensitivity analysis reveals that this uncertainty is small because the photocatalyst, solvent, and ion are held at parity in these comparative measurements. A proof-of-principle example is provided for halide stabilization by a dicationic ligand coordinated to an Ir photocatalyst. The use of an Ir photocatalyst enabled facile oxidation of both stabilized and unstabilized halides without the ligand-loss chemistry that plagues the most potent Ru polypyridyl photooxidants. The kinetic data and analysis reveal that the magnitude of K_{eq} was correlated with $\Delta E^{\circ\prime}(X^{\bullet/-})$, but that additional noncovalent interactions were necessary to rationalize the stabilization of iodide relative to bromide.

RESULTS

Photophysical and Electrochemical Characterization

The photocatalyst $[Ir(dF\text{-}(CF_3)\text{-}ppy)_2(tmam)]^{3+}$ (tmam = [4,4′-bis[(trimethylamino)methyl]-2,2′-bipyridine]$^{2+}$), abbreviated Ir-tmam, displayed spectroscopic properties typical for iridium complexes with two cyclometallating ligands and one bipyridyl-type ligand.[30] The excited state displays broad room temperature photoluminescence (PL) with a maximum at 570 nm (Figure S1). Pulsed-light excitation with 465 nm light in argon-saturated acetonitrile generated a long-lived excited state that decayed by first-order kinetics with a lifetime $\tau_o = 1.0\ \mu s$. In cyclic voltammetry experiments, Ir-tmam exhibited an irreversible reduction $E^{\circ\prime}(Ir^{3+/2+}) \approx -1.32$ V versus $Fc^{+/0}$ in an acetonitrile electrolyte solution. Irreversible reduction of complexes containing tmam ligands has been previously observed and attributed to deamination of the reduced ligand.[31−36] The Gibbs free energy stored in the excited state, $\Delta G_{es} = 2.55$ eV, was extracted from the blue edge of the PL spectrum. The lack of reversible electrochemistry precluded exact determination of the excited-state reduction $[E^{\circ\prime}(Ir^{3+*/2+})]$, but was estimated to be ∼1.2 V versus $Fc^{+/0}$ (eq 2).

$$E^{\circ\prime}(Ir^{3+*/2+}) = E^{\circ\prime}(Ir^{3+/2+}) + \Delta G_{es} \quad (2)$$

NMR Ion-Pairing Titrations

^{1}H NMR spectroscopy was used to determine the location of halide association with Ir-tmam and the corresponding equilibrium constants. Titration of tetrabutylammonium iodide (TBAI) into a CD_3CN solution of Ir-tmam revealed the most

https://doi.org/10.1021/jacsau.2c00088
JACS Au 2022, 2, 985−995

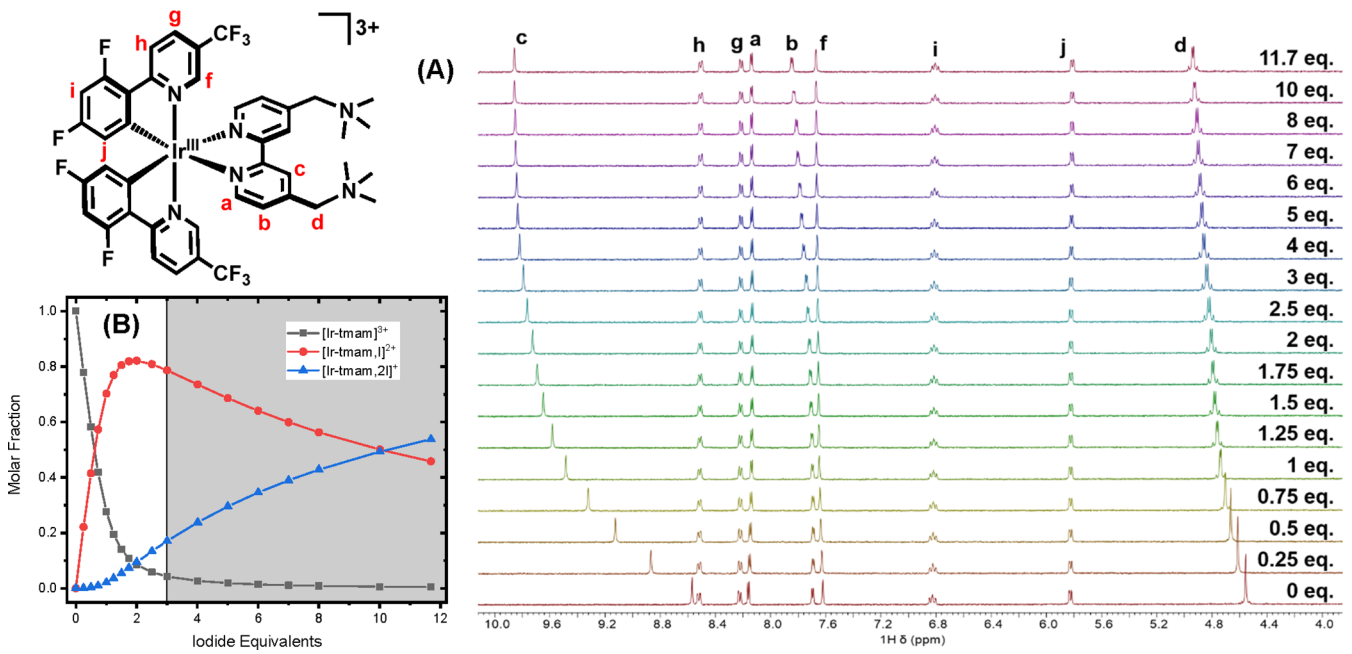

Figure 1. (A) ^{1}H NMR titration of TBAI into a solution of Ir-tmam in acetonitrile with the indicated equivalents of iodide. (B) Molar fraction of "free" $[Ir\text{-}tmam]^{3+}$, the singly ion-paired species $[Ir\text{-}tmam,I]^{2+}$, and doubly ion-paired species $[Ir\text{-}tmam,2I]^{+}$ as a function of iodide equivalents added. The unshaded portion of the plot represents the concentration region that PL measurements were performed.

significant chemical shift change for the 3,3′ tmam hydrogens (Figure 1, labeled "c") that saturated by ∼3 equiv I^-. This suggests that the initial iodide ion pairing occurred with a strong interaction localized near the most acidic 3,3′ bipyridyl hydrogens, consistent with previous reports of halide binding with ruthenium-based polypyridyl complexes.[37] Downfield shifts were also observed for the methylene-tmam protons (labeled "d") throughout the titration, as well as small changes in the 5,5′ tmam resonance (labeled "b") at higher concentrations of iodide. The inflection point in the latter change in chemical shift suggested that a second, less favorable ion pair formed in the presence of excess iodide. Changes in chemical shift were fit to a 1:2 (Ir-tmam/iodide) binding model using the Supramolecular fitting software to extract the ion-pairing equilibrium constants.[38] The first and second association constants with iodide were determined to be K_{11} = 1.00 ± 0.02 × 10^4 M^{-1} and K_{12} = 1.19 ± 0.03 × 10^2 M^{-1}, respectively.[38−40]

Titration of tetrabutylammonium bromide (TBABr) into a CD_3CN solution of Ir-tmam (Figure S5) induced chemical shift changes that were similar to the behavior of TBAI. The most significant change was again observed for the 3,3′ tmam hydrogens, which saturated by ∼2 equiv Br^-. The more rapid and significant change in chemical shift observed for Br^- relative to I^- suggested a higher binding affinity for the smaller halide, which is consistent with prior studies.[22] The presence of an inflection point in the chemical shift changes to the 5,5′ tmam resonances at higher $[Br^-]$ indicated that a second halide binding occurred with excess bromide. The first and second association constants with bromide were determined to be K_{11} = 7 ± 2 × 10^4 M^{-1} and K_{12} = 3.1 ± 0.3 × 10^2 M^{-1}, respectively.[38−40]

The speciation of Ir-tmam ion pairs as a function of halide equivalents added is shown in Figures 1B and S6 for iodide and bromide, respectively. When ∼2 equiv of iodide was added, the singly ion-paired species $[Ir\text{-}tmam,I]^{2+}$ was at its highest concentration and accounted for >80% of the Ir species present. The doubly ion-paired species $[Ir\text{-}tmam,2I]^{+}$ was not the dominant species until >10 equiv of iodide was added. For bromide, the singly ion-paired species $[Ir\text{-}tmam,Br]^{2+}$ reached its highest concentration at ∼1.75 equiv (>85% of the Ir species present) and the doubly ion-paired species $[Ir\text{-}tmam,2Br]^{+}$ was not the dominant species until >5 equiv.

PL and Stern−Volmer Analysis

PL titrations were performed from 0 to <3 equiv of halide (unless otherwise stated), such that $[Ir\text{-}tmam]^{3+}$ and $[Ir\text{-}tmam,X]^{2+}$ were the dominant species in solution over this concentration range (Figures 1B and S6, unshaded). Precluding substantial contribution of the doubly ion-paired species ensured that the kinetic data could be modeled by considering only the two dominant species.

Titration of TBAI or TBABr quenched the steady-state PL intensity (PLI) of Ir-tmam (Figures S7 and S8). Stern−Volmer plots of PLI_0/PLI versus halide concentration displayed upward curvature that is commonly attributed to the presence of a static quenching mechanism (Figure 2c).[41] A modified Stern−Volmer expression (see the Supporting Information) has traditionally been used to model data where combined dynamic and static quenching is operative and assumes that the nonluminescent ground-state adduct is responsible for the static component.[41] For iodide quenching, the modified Stern−Volmer expression provided an estimate of K_{eq} = 8600 ± 200 M^{-1} that is in fair agreement with the K_{eq} determined by NMR, but this was not the case for bromide. In this study, the assumption that the ground-state adduct, $[Ir\text{-}tmam,X]^{2+}$, was nonluminescent is invalid, particularly when X = Br, as is presented below. A ∼9 nm blue shift in the PL λ_{max} was also observed during halide titrations. This hypsochromic shift indicated that approximately ∼35 meV more energy was stored in the excited state, ΔG_{es}, of the ion-paired $[Ir\text{-}tmam,X]^{2+*}$ complex. There was no evidence that halide association impacted the MLCT character of the excited state,

https://doi.org/10.1021/jacsau.2c00088
JACS Au 2022, 2, 985−995

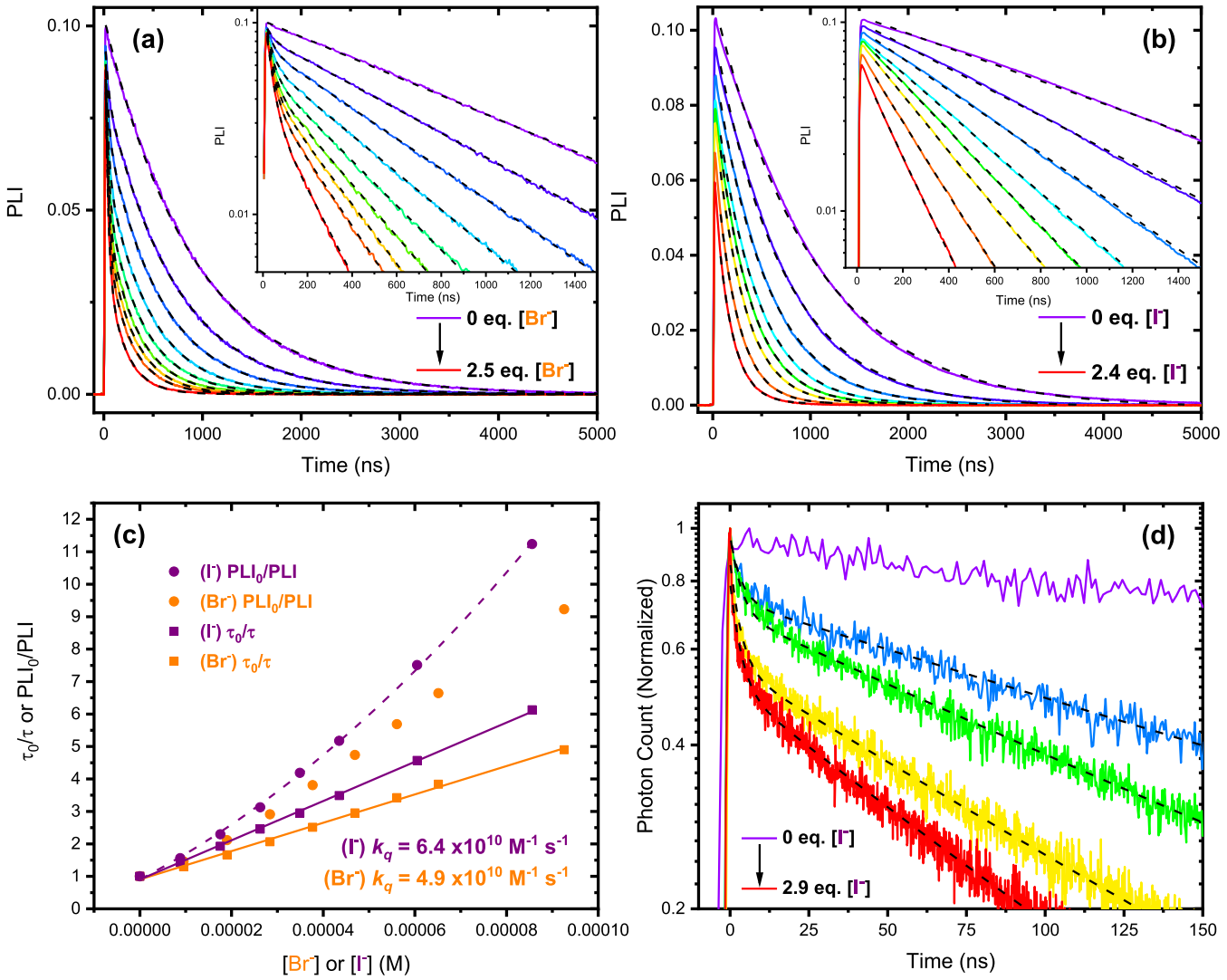

Figure 2. (a) Time-resolved PL with increasing [Br^-] and biexponential fits overlaid (black dashes). The inset is plotted on a log scale to demonstrate the biexponential decay of the excited state. (b) Time-resolved PL with increasing [I^-] and monoexponential fits superimposed (black dashes) with a log scale shown as an inset. (c) Stern–Volmer plot of PLI_0/PLI or τ_0/τ as a function of [Br^-] or [I^-] with fits overlaid. (d) TCSPC PL plotted on a log scale with increasing [I^-] and biexponential fits superimposed (black dashes).

given that halide addition did not affect the shape or full width at half maximum of the normalized steady-state PL. The irreversible nature of the Ir-tmam reduction precluded experiments to measure any shift in the ground-state reduction potential when ion-paired with iodide or bromide. However, previous studies on a related polypyridyl complex with a similar halide binding affinity reported a 40 mV cathodic shift in the first reduction potential upon halide ion pairing.[22] Given that changes to $E^{\circ\prime}(Ir^{3+/2+})$ and ΔG_{es} are similar in magnitude but in opposing directions, a negligible shift in $E^{\circ\prime}(Ir^{3+*/2+})$ is anticipated for the ion-paired complex (eq 2).

Pulsed-laser experiments with approximately 10 ns time resolution revealed that titrations with iodide quenched the Ir-tmam excited-state lifetime and led to a decrease in the initial PL amplitude (α), indicative of dynamic and static quenching, respectively (Figure 2b).[42,43] These data were well described by a first-order kinetic model with monoexponential decay observed at all iodide concentrations investigated (eq 3). A quenching rate constant resulting from freely diffusing iodide was extracted from the linear τ_0/τ plot, $k_q = 6.4 \times 10^{10}$ M^{-1} s^{-1}, which was reproducibly measured to two significant figures. The static component was attributed to the stabilized iodide that quenched the Ir-tmam excited state within the instrument response time of 10 ns.

$$\text{PLI}\,(t) = \alpha(\exp(-t/\tau)) \tag{3}$$

Iodide titrations were subsequently performed with a time-correlated single photon counting (TCSPC) PL assay in order to achieve picosecond resolution of the Ir-tmam quenching processes. On this time scale, biexponential kinetics were observed, consistent with two competitive quenching processes (eq 4, Figure 2d).

$$\text{PLI}\,(t) = \alpha_1\left(\exp\left(-\frac{t}{\tau}\right)\right) + \alpha_2\left(\exp\left(-\frac{t}{\tau_s}\right)\right) \tag{4}$$

The first quenching mechanism was first order in [I^-], where Stern–Volmer analysis revealed a quenching rate constant of 6.3×10^{10} M^{-1} s^{-1} (Figure S9), consistent with a diffusional quenching mechanism in excellent agreement with the rate constant determined from nanosecond pulsed-laser experiments. The second quenching process was rapid with a lifetime

https://doi.org/10.1021/jacsau.2c00088
JACS Au 2022, 2, 985–995

Scheme 2. Two Competitive Electron-Transfer Quenching Pathways[a]

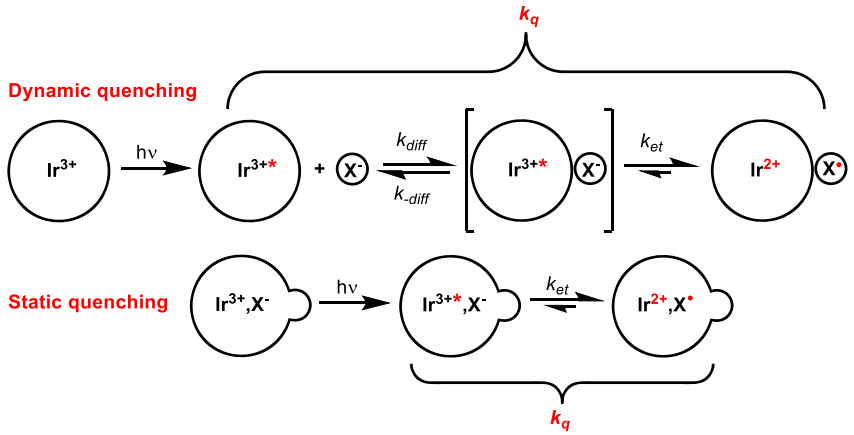

[a]Dynamic quenching involves diffusional encounters of the halide with the excited state. Static quenching occurs when the halide associates with the stabilizing group in the ground state.

of τ_s = 3.2 ns that was independent of [I^-], but was only observed once iodide was added. This short-lived excited-state species was attributed to [Ir-tmam,I]$^{2+}$*, where rapid quenching occurred within the adduct that was preassociated in the ground state. This "static" quenching process manifested as a decrease in the initial amplitude in the previously described nanosecond pulsed-laser experiments but was able to be time-resolved using TCSPC.

Nanosecond pulsed-laser experiments provided sufficient time resolution to reveal excited-state quenching of Ir-tmam by bromide that was well described by a biexponential kinetic model with increasing [Br^-] (eq 4). Analogous to the picosecond kinetic data for iodide, the biexponential excited-state decay revealed one component with a lifetime that was bromide concentration-dependent, consistent with diffusional quenching, and a second lifetime, τ_s = 29 ns, that was independent of bromide concentration (Figure 2a). Stern–Volmer analysis of the diffusional quenching lifetimes showed a linear dependence on bromide concentration, from which a quenching rate constant of $k_q = 4.9 \times 10^{10}$ M^{-1} s^{-1} was extracted (Figure 2c).

The assignment of both quenching mechanisms as electron-transfer processes is based on prior work that has demonstrated reductive quenching of similar Ir photocatalysts by halides,[16,44−46] as well as the important consideration that there is no energetic overlap between the Ir-tmam PL and X^- absorbance to enable alternative energy transfer quenching mechanisms. The assignment of a reductive quenching mechanism was confirmed by observation of the reduced photocatalyst and oxidized halide photoproduct by nanosecond transient absorption spectroscopy (Figure S10).

Marcus Theory Analysis

The dynamic quenching process proceeded through a composite mechanism where the first step was the diffusional encounter of the excited state, Ir-tmam^{3+}*, with an unstabilized, freely diffusing halide, X^-, to form an "encounter complex", subsequently followed by electron transfer (Scheme 2). Application of the time-honored steady-state approximation to the encounter complex and correction for diffusion in acetonitrile ($k_{diff} = 1.02 \times 10^{11}$ M^{-1} s^{-1} for Ir-tmam^{3+}* and I^- under the reported experimental conditions) allowed the electron-transfer rate constant, k_{et}, to be extracted from the observed quenching rate constant, k_q (see Supporting Information).[16,47−54] The static quenching observed with the stabilized halide occurred by direct excitation of a ground-state halide photocatalyst adduct, [Ir-tmam,X]$^{2+}$. Because the halide was associated with the photocatalyst prior to excitation, the kinetics were independent of [X^-] and there was no diffusional step; the measured kinetics reported directly on the elementary electron-transfer step, $k_{et} = k_q = 1/\tau_s$.

The electron-transfer rate constants report directly on the driving force for electron transfer, $-\Delta G^\circ_{et}$, which were determined through semiclassical Marcus theory. Within the Marcus expression (eq 5), the reorganization energy, λ = 1 eV,[55−61] and pre-exponential frequency factor, $A = 10^{11}$ s^{-1},[54,62,63] were assumed to be at parity for both the stabilized and diffusional electron transfer. The pre-exponential factor contains the electronic coupling matrix element, H_{ab}, which is expected to be small for bimolecular reactions. A sensitivity analysis was performed where the values for λ and H_{ab} were varied one at a time over physically realistic values of 0.8 to 1.2 eV and 10 to 100 cm^{-1}, respectively, to estimate the uncertainties in $\Delta E^{\circ\prime}(X^{\bullet/-})$ of ±24 meV for bromide and ±13 meV for iodide. Quenching rate constants, electron-transfer rate constants, and the driving forces for electron transfer are tabulated in Table 1.

$$k_{et} = \frac{2\pi}{\hbar}|H_{AB}|^2 \frac{1}{\sqrt{4\pi\lambda k_B T}} \exp\left(-\frac{(\lambda + \Delta G^\circ)^2}{4\lambda k_B T}\right) = A \exp\left(-\frac{(\lambda + \Delta G^\circ)^2}{4\lambda k_B T}\right) \quad (5)$$

Table 1. Kinetic and Thermodynamic Values for Quenching by Stabilized and Unstabilized Bromide and Iodide

	Br^- (unstabilized)	Br^- (stabilized)	I^- (unstabilized)	I^- (stabilized)
k_q (M^{-1} s^{-1})	4.9×10^{10}		6.4×10^{10}	
k_{et} (s^{-1})	4.1×10^8	3.4×10^7	8.0×10^8	3.1×10^8
$-\Delta G^\circ_{et}$ (meV)	250	95	300	230

https://doi.org/10.1021/jacsau.2c00088
JACS Au 2022, 2, 985−995

Scheme 3. Competitive Excited-State Electron Transfers from a Stabilized Bromide (Left) and a Solvated Bromide (Right)

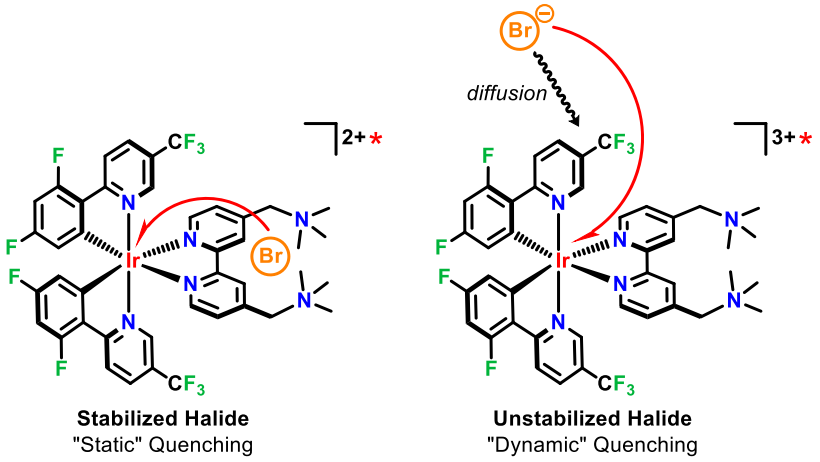

DISCUSSION

A new iridium photocatalyst was synthesized featuring a dicationic bipyridyl ligand (tmam). Visible light excitation of Ir-tmam generated a long-lived ∼1 μs photoluminescent excited state. Kinetic measurements revealed that two competitive excited-state quenching mechanisms were operative for either bromide or iodide. These mechanisms were attributed to dynamic electron transfer from a freely diffusing, unstabilized halide and a static mechanism with a stabilized halide sequestered by the photocatalyst (Scheme 3). The concurrent oxidation of stabilized and unstabilized halides provided a novel opportunity to analyze the kinetic data with semiclassical Marcus theory to compare electron-transfer driving forces and, ultimately, quantify the stabilization of these ions toward oxidation through noncovalent interactions under experimentally relevant conditions. Below we discuss the implications of this work and assumptions inherent to this analysis beginning with the molecular structure of the stabilized halide and photocatalyst and ending with previously described approaches to quantify ion stabilization.

The tmam ligand was chosen as previous research with ruthenium-based photocatalysts has shown the presence of a "halide-binding pocket", where a single halide ion is stabilized by both cationic quaternary amines and H-bonding to hydrogen atoms on the bipyridyl ligand.[12,21,37,64−67] ^{1}H NMR titrations with Ir-tmam are in good agreement with these prior studies and provide equilibrium constants of 7×10^4 and 1×10^4 M^{-1} for Br^- and I^-, respectively. We note that a second, weaker ion pair formed in the presence of excess halides ($K_{12} \approx 10^2$ M^{-1}) that was intentionally precluded from the kinetic analysis. An important observation from this and prior studies is that the 2-fold rotational symmetry axis along the plane defined by tmam and the metal center was maintained throughout the halide titrations, indicating that a single halide resided within the plane of the bipyridine ligand stabilized equally by both ammonium groups. Despite the structurally analogous ion pairing, it is interesting to note that prior work with ruthenium-based photocatalysts found that tmam stabilized the sequestered halide to an extent that it inhibited electron transfer even from iodide—the easiest halide to oxidize—yet the photocatalyst was still quenched diffusionally by unstabilized halides.[21] This is in marked contrast to this report where both quenching pathways were observed, behavior attributed to the larger driving force for halide oxidation by the more potent iridium-based photooxidant reported herein.

While the location of the stabilized halide is reasonably well understood, the same is not true for the unstabilized halide in solution. The degree of halide solvation is usually unknown, particularly in nonaqueous environments, which presents a major challenge for estimating ion stabilization through computational methods or thermochemical cycles.[68] A large body of bimolecular (or ionic) electron-transfer data reported over the past decades indicate that electron transfer occurs after diffusional encounters within a solvent cage that is often called an encounter complex. While the structure and solvation within the encounter complex are typically unknown and difficult to quantify experimentally, an advantage of the approach described herein is the comparative nature of the kinetic data that directly reports on the relative driving force for oxidation of the stabilized and unstabilized ions. Thus, comparison of these values is expected to provide a direct measure of $\Delta E^{\circ\prime}(X^{\bullet/-})$ under experimentally relevant conditions without *a priori* knowledge of the innumerable factors that may impact stabilization.

On the other hand, inherent to this comparative kinetic approach is the assumption that the electronic coupling (H_{ab}) and reorganization energy (λ) within this encounter complex are the same as that for the stabilized ion. These parameters are discussed below as this assumption is important and can be tested with a larger body of experimental data. The reorganization energy is typically taken as a sum of inner- and outer-sphere contributions. The inner-sphere contributions involve changes in bond angles and lengths, which are absent for the halides and minimal for these MLCT excited states. Hence, the reorganization energy is determined mainly by the solvent and a typical value of 1 eV in polar solvents was adopted. Previous analysis of halide charge transfer to solvent transitions revealed that λ is not highly sensitive to the halide identity.[69] Nevertheless, it is prudent to emphasize that the solvent coordination number for halides, and ions in general, is largely unknown,[70] so it is difficult to say with certainty that a common reorganization energy is completely appropriate for stabilized and unstabilized halides.

The electronic coupling is directly related to the overlap of the donor−acceptor wavefunctions at the instant of electron transfer. For these $18e^-$ $d\pi^6$ photocatalysts, the formation of a seven-coordinate encounter complex is highly unlikely and unprecedented, indicating that electron transfers proceed

https://doi.org/10.1021/jacsau.2c00088
JACS Au 2022, 2, 985−995

through outer-sphere mechanisms. Hence, electron transfer from the stabilized halide occurs by tunneling through the halide-sequestering tmam ligand. While direct contact between the donor and acceptor promotes electronic coupling,[71] the tmam ligand is formally reduced in the excited state and therefore does not provide strong coupling to the acceptor orbital predominantly localized on the metal and cyclometallating ligands.[72,73] Indeed, prior reductive quenching studies reported no measurable kinetic difference when an electron donor was covalently tethered proximal or distal to the ligand formally reduced in the excited state.[74]

For the diffusional electron transfer, it is likely that the most significant wavefunction overlap occurs when X^- is near the cyclometallating ligands of Ir-tmam^{3+*}. In the absence of a halide-sequestering ligand, previous molecular dynamics simulations in acetonitrile solutions indicate that polypyridyl photocatalysts form solvent-shared interactions with halides, suggesting that direct contact of the halide and photocatalyst is not favored and thus unlikely to lead to enhanced electronic coupling.[75] Therefore, like most bimolecular electron-transfer reactions, the electronic coupling is expected to be small for both electron transfers. Consistent with this assertion, recent studies with similar iridium photocatalysts reported that a common value for λ and H_{ab} was suitable to fit a Marcus curve for a series of structurally disparate electron donors, including neutral organic donors as well as anionic halides.[44]

The remaining unknown parameter within the Marcus equation, ΔG°_{et}, depends on the excited-state reduction potential of the acceptor, $E^{\circ\prime}(Ir^{3+*/2+})$, and the reduction potential of the donor, $E^{\circ\prime}(X^{\bullet/-})$. Given that $E^{\circ\prime}(Ir^{3+*/2+})$ is largely insensitive to halide association under the relevant experimental conditions, it is reasonable to assign the difference in ΔG°_{et} measured for oxidation of the stabilized and unstabilized halides as a direct perturbation to $E^{\circ\prime}(X^{\bullet/-})$. Therefore, the kinetic data indicate that Ir-tmam stabilizes bromide and iodide by approximately $\Delta E^{\circ\prime}(Br^{\bullet/-}) = 150 \pm 24$ meV and $\Delta E^{\circ\prime}(I^{\bullet/-}) = 67 \pm 13$ meV, respectively (Table 2).

Table 2. Ground-State Equilibrium Values and Perturbation to Halogen Reduction Potential from Ion Stabilization

	bromide	iodide
K_{eq} (M^{-1})	$7 \pm 2 \times 10^4$	$1 \pm 0.02 \times 10^4$
$-\Delta G^\circ_{eq}$ (meV)	290	240
$\Delta E^{\circ\prime}(X^{\bullet/-})$ (mV)	150 ± 24	67 ± 13

These values for stabilization toward oxidation are qualitatively consistent with the measured equilibrium constants, which corresponded to $-\Delta G^\circ_{eq} = 290$ and 240 meV with bromide and iodide, respectively (eq 1). However, the fact that the shift in $E^{\circ\prime}(X^{\bullet/-})$ for iodide is less than 1/2 that of bromide could not have been ascertained from this ground-state equilibrium data. Instead, one might have naively expected $\Delta E^{\circ\prime}(X^{\bullet/-})$ to be within 20% of each other. It is therefore of interest to speculate why $\Delta E^{\circ\prime}(Br^{\bullet/-})$ is more than twice that of iodide.

In the hypothetical scenario presented in the Introduction, it was stated that if the only relevant consideration was a Coulombic attraction, then oxidation of X^- to $X^\bullet$ would eliminate any stabilizing interaction. A survey of the literature quickly reveals this to be incorrect. A relevant example that contradicts this hypothetical scenario is the substantial body of work that has studied the stabilizing interaction of halogen atoms with aromatic systems.[13,15,76−87] Not only does this imply that there are more interactions to consider than Coulombic attraction, it also introduces the notion that the impact of "stabilization" on formal reduction potentials must consider the electron-transfer products as well as the reactants. It is possible (if not probable) that formation of a π-halogen adduct concomitant with electron transfer could stabilize the product pair, thereby altering the thermodynamic driving force for halide oxidation. Prior DFT calculations have estimated that formation of a $Br^\bullet$-benzene adduct provided up to 220 meV of thermodynamic stabilization.[80] It is prudent to note, however, that at the instant of electron transfer, it is unlikely that the halogen atom would be positioned in an orientation relative to the aromatic ligands on the photocatalyst that would provide the maximal stabilization that has been predicted by theory.[80] Nevertheless, the results reported here suggest that particularly for the highly polarizable iodine atom, stabilizing interactions may be operative without strict geometric requirements. The extent to which such an interaction may be an important consideration for oxidation of the sequestered versus diffusing halide is not yet known but serves as an example that demonstrates how ground state equilibria may provide an incomplete picture of how noncovalent interactions impact reduction potentials. In particular, it is encouraging that the predicted magnitude of halogen atom stabilization is similar to the $-\Delta G^\circ_{eq}$ reported herein, suggesting that an appropriately designed photocatalyst could offset the halide stabilization necessary for selective sequestration by commensurate stabilization of the halogen atom.

Lastly, it is important to place this approach in the context of some previous studies that have successfully utilized kinetic data to determine thermodynamic parameters related to ion pairing in various contexts. Time-resolved fluorescence measurements have been used to determine that ion pairs in a frozen glass were destabilized by ∼800 meV relative to polar solvents.[88,89] However, it is not clear from these studies how the formal reduction potentials of the donor or the acceptor were impacted by ion pairing. More recently, a novel method to determine electrolyte-free reduction potentials has been developed using pulse radiolysis that accounts for the free-energy change for ion pairing with bulk electrolyte solutions. While ostensibly similar to the work presented here, this prior work is relevant to systems where ion pair formation happens in concert with electron transfer. An advantage to the method presented here is that $\Delta E^{\circ\prime}(X^{\bullet/-})$ can be measured directly from comparison of the rate constants for oxidation of the halide that is stabilized (ion paired) and in solution. Moreover, the use of luminescence measurements makes this approach amenable to most academic laboratories without the need for specialized radiation sources.

CONCLUSIONS

A new kinetic approach for determination of the change in the formal reduction potential imparted by environmental stabilization is described and applied to bromine and iodine atoms. Light excitation of a photocatalyst initiated competitive quenching kinetics by a stabilized halide ion and a solvated halide ion. Stabilization by a photocatalyst with two cationic ammonium groups and H-bond donors was shown to result in a significant increase in the formal reduction potentials relative to the solvated species. The collective data reported herein revealed important interrelated conclusions that were not evident in previously published articles.

https://doi.org/10.1021/jacsau.2c00088
JACS Au 2022, 2, 985−995

The association equilibrium constants for ion sequestration were a poor indicator of the magnitude of the reduction potential shift, but qualitatively predicted that the stabilized bromide was more difficult to oxidize than the stabilized iodide relative to their solvated ion counterparts. The ^{1}H NMR titrations revealed that iodide and bromide were stabilized by the same noncovalent interactions within the dicationic ligand. The K_{eq} value for bromide was a factor of 7 larger than that for iodide, yet the shifts in the formal reduction potentials differed by a factor of 2. While K_{eq} values are often the only quantitative measure of ion stabilization available experimentally, their use as a predictor of perturbations to formal reduction potentials should be done with extreme caution.

The assumption that Coulombic interactions alone are the only noncovalent interaction of significance must be carefully considered. If stabilization of the halogen atom was nonexistent, then the simple free energy consideration of Scheme 1a would have provided a means to predict the change in reduction potential of the stabilized halide ion. The experimentally measured K_{eq} values did report on the Columbic interactions of the halide ions as well as the weaker hydrogen bonding interactions with the tricationic photocatalyst; however, assuming K_{eq} was zero for the neutral halogen atom resulted in shifts in the formal potentials that were outside the range of error determined through the sensitivity analysis.

Studies of photocatalysts with fewer (or additional) ionic groups as well as alternative groups capable of H-bonding or other noncovalent interactions will provide greater insights into environmental stabilization of redox reactions relevant to chemistry and biology. Of relevance to this particular study is the goal of designing materials that preferentially sequester a single analyte from a complex mixture for subsequent light-driven redox chemistry, such as the selective oxidation of chloride ions in sea water. The data herein reveal that sequestration necessarily stabilizes the analyte of interest and that this need not necessarily lead to a large unfavorable shift in the formal reduction potential if the redox partner of the analyte can also be stabilized significantly. Indeed, while speculative, the increased stabilization of the iodine atom is likely responsible for the smaller increase in $\Delta E^{\circ\prime}(I^{\bullet/-})$ relative to $\Delta E^{\circ\prime}(Br^{\bullet/-})$. Hence, future research on functional groups that stabilize both halves of the redox couple, here the atom and the ion, is likely to provide greater insights into ion and radical stabilization necessary for real-world applications.

■ ASSOCIATED CONTENT

Supporting Information

The Supporting Information is available free of charge at https://pubs.acs.org/doi/10.1021/jacsau.2c00088.

Experimental details, methods, and materials; UV−Vis, ^{1}H, ^{13}C, and ^{19}F NMR characterization of Ir-tmam; ^{1}H NMR halide binding titration experiments; steady-state PL for halide titrations; TCSPC Stern−Volmer plot; and transient absorption spectrum (PDF)

■ AUTHOR INFORMATION

Corresponding Author

Gerald J. Meyer − *Department of Chemistry, University of North Carolina at Chapel Hill, Chapel Hill, North Carolina 27599-3290, United States;* orcid.org/0000-0002-4227-6393; Email: gjmeyer@email.unc.edu

Author

Alexander M. Deetz − *Department of Chemistry, University of North Carolina at Chapel Hill, Chapel Hill, North Carolina 27599-3290, United States*

Complete contact information is available at: https://pubs.acs.org/10.1021/jacsau.2c00088

Author Contributions

The manuscript was written through contributions of both authors. A.M.D. completed all the experimental studies. Both authors have given approval to the final version of the manuscript.

Notes

The authors declare no competing financial interest.

■ ACKNOWLEDGMENTS

The research was supported by the National Science Foundation under Award CHE-1465060. A.M.D. acknowledges the Department of Chemistry at the University of North Carolina for providing individual funding through the Eliel Fellowship. This work made use of the Edinburgh FLS920 instrument in the CHASE Instrumentation Facility established by the Center for Hybrid Approaches in Solar Energy to Liquid Fuels, an Energy Innovation Hub funded by the U.S. Department of Energy, Office of Science, and Office of Basic Energy Sciences under Award Number DE-SC0021173. We also thank Renato Sampaio and Ludovic Troian-Gautier for their experimental and synthetic suggestions.

■ REFERENCES

(1) Verschueren, K. H. G.; Seljée, F.; Rozeboom, H. J.; Kalk, K. H.; Dijkstra, B. W. Crystallographic Analysis of the Catalytic Mechanism of Haloalkane Dehalogenase. *Nature* **1993**, *363*, 693−698.

(2) Lightstone, F. C.; Zheng, Y.-J.; Bruice, T. C. Molecular Dynamics Simulations of Ground and Transition States for the S(N)2 Displacement of Cl- from 1,2-Dichloroethane at the Active Site of Xanthobacter Autotrophicus Haloalkane Dehalogenase. *J. Am. Chem. Soc.* **1998**, *120*, 5611−5621.

(3) Kennes, C.; Pries, F.; Krooshof, G. H.; Bokma, E.; Kingma, J.; Janssen, D. B. Replacement of Tryptophan Residues in Haloalkane Dehalogenase Reduces Halide Binding and Catalytic Activity. *Eur. J. Biochem.* **1995**, *228*, 403−407.

(4) Boháč, M.; Nagata, Y.; Prokop, Z.; Prokop, M.; Monincová, M.; Tsuda, M.; Koca, J.; Damborský, J. Halide-Stabilizing Residues of Haloalkane Dehalogenases Studied by Quantum Mechanic Calculations and Site-Directed Mutagenesis. *Biochemistry* **2002**, *41*, 14272−14280.

(5) Hasan, K.; Gora, A.; Brezovsky, J.; Chaloupkova, R.; Moskalikova, H.; Fortova, A.; Nagata, Y.; Damborsky, J.; Prokop, Z. The Effect of a Unique Halide-Stabilizing Residue on the Catalytic Properties of Haloalkane Dehalogenase DatA from Agrobacterium Tumefaciens C58. *FEBS J.* **2013**, *280*, 3149−3159.

(6) Schindler, J. F.; Naranjo, P. A.; Honaberger, D. A.; Chang, C.-H.; Brainard, J. R.; Vanderberg, L. A.; Unkefer, C. J. Haloalkane Dehalogenases: Steady-State Kinetics and Halide Inhibition. *Biochemistry* **1999**, *38*, 5772−5778.

(7) Schanstra, J. P.; Janssen, D. B. Kinetics of Halide Release of Haloalkane Dehalogenase: Evidence for a Slow Conformational Change. *Biochemistry* **1996**, *35*, 5624−5632.

(8) Brak, K.; Jacobsen, E. N. Asymmetric Ion-Pairing Catalysis. *Angew. Chem., Int. Ed.* **2013**, *52*, 534−561.

(9) Raheem, I. T.; Thiara, P. S.; Peterson, E. A.; Jacobsen, E. N. Enantioselective Pictet-Spengler-Type Cyclizations of Hydroxylactams: H-Bond Donor Catalysis by Anion Binding. *J. Am. Chem. Soc.* **2007**, *129*, 13404−13405.
(10) Reisman, S. E.; Doyle, A. G.; Jacobsen, E. N. Enantioselective Thiourea-Catalyzed Additions to Oxocarbenium Ions. *J. Am. Chem. Soc.* **2008**, *130*, 7198−7199.
(11) Taylor, M. S.; Tokunaga, N.; Jacobsen, E. N. Enantioselective Thiourea-Catalyzed Acyl-Mannich Reactions of Isoquinolines. *Angew. Chem., Int. Ed.* **2005**, *44*, 6700−6704.
(12) Troian-Gautier, L.; Turlington, M. D.; Wehlin, S. A. M.; Maurer, A. B.; Brady, M. D.; Swords, W. B.; Meyer, G. J. Halide Photoredox Chemistry. *Chem. Rev.* **2019**, *119*, 4628−4683.
(13) Hwang, S. J.; Powers, D. C.; Maher, A. G.; Anderson, B. L.; Hadt, R. G.; Zheng, S.-L.; Chen, Y.-S.; Nocera, D. G. Trap-Free Halogen Photoelimination from Mononuclear Ni(III) Complexes. *J. Am. Chem. Soc.* **2015**, *137*, 6472−6475.
(14) Powers, D. C.; Hwang, S. J.; Zheng, S.-L.; Nocera, D. G. Halide-Bridged Binuclear HX-Splitting Catalysts. *Inorg. Chem.* **2014**, *53*, 9122−9128.
(15) Hwang, S. J.; Anderson, B. L.; Powers, D. C.; Maher, A. G.; Hadt, R. G.; Nocera, D. G. Halogen Photoelimination from Monomeric Nickel(III) Complexes Enabled by the Secondary Coordination Sphere. *Organometallics* **2015**, *34*, 4766−4774.
(16) Deetz, A. M.; Troian-Gautier, L.; Wehlin, S. A. M.; Piechota, E. J.; Meyer, G. J. On the Determination of Halogen Atom Reduction Potentials with Photoredox Catalysts. *J. Phys. Chem. A* **2021**, *125*, 9355−9367.
(17) Liu, Y.; Zhao, W.; Chen, C. H.; Flood, A. H. Chloride Capture Using a c−h Hydrogen Bonding Cage. *Science* **2019**, *365*, 159−161.
(18) Pedersen, C. J. Cyclic Polyethers and Their Complexes with Metal Salts. *J. Am. Chem. Soc.* **1967**, *89*, 7017−7036.
(19) Pedersen, C. J. Cyclic Polyethers and Their Complexes with Metal Salts. *J. Am. Chem. Soc.* **1967**, *89*, 2495−2496.
(20) Dietrich, B.; Lehn, J. M.; Sauvage, J. P. Les Cryptates. *Tetrahedron Lett.* **1969**, *10*, 2889−2892.
(21) Wehlin, S. A. M.; Troian-Gautier, L.; Sampaio, R. N.; Marcélis, L.; Meyer, G. J. Ter-Ionic Complex That Forms a Bond Upon Visible Light Absorption. *J. Am. Chem. Soc.* **2018**, *140*, 7799−7802.
(22) Troian-Gautier, L.; Beauvilliers, E. E.; Swords, W. B.; Meyer, G. J. Redox Active Ion-Paired Excited States Undergo Dynamic Electron Transfer. *J. Am. Chem. Soc.* **2016**, *138*, 16815−16826.
(23) Bird, M. J.; Iyoda, T.; Bonura, N.; Bakalis, J.; Ledbetter, A. J.; Miller, J. R. Effects of Electrolytes on Redox Potentials through Ion Pairing. *J. Electroanal. Chem.* **2017**, *804*, 107−115.
(24) Bird, M. J.; Pearson, M. A.; Asaoka, S.; Miller, J. R. General Method for Determining Redox Potentials without Electrolyte. *J. Phys. Chem. A* **2020**, *124*, 5487−5495.
(25) Mani, T.; Grills, D. C.; Miller, J. R. Vibrational Stark Effects to Identify Ion Pairing and Determine Reduction Potentials in Electrolyte-Free Environments. *J. Am. Chem. Soc.* **2015**, *137*, 1136−1140.
(26) Rehm, D.; Weller, A. Kinetik Und Mechanismus Der Elektronübertragung Bei Der Fluoreszenzlöschung in Acetonitril. *Ber. Bunsenges. Phys. Chem.* **1969**, *73*, 834−839.
(27) Rehm, D.; Weller, A. Kinetics of Fluorescence Quenching by Electron and H-Atom Transfer. *Isr. J. Chem.* **1970**, *8*, 259−271.
(28) Savéant, J.-M. Effect of Ion Pairing on the Mechanism and Rate of Electron Transfer. Electrochemical Aspects. *J. Phys. Chem. B* **2001**, *105*, 8995−9001.
(29) Piechota, E. J.; Meyer, G. J. Introduction to Electron Transfer: Theoretical Foundations and Pedagogical Examples. *J. Chem. Educ.* **2019**, *96*, 2450−2466.
(30) Diluzio, S.; Mdluli, V.; Connell, T. U.; Lewis, J.; Vanbenschoten, V.; Bernhard, S. High-Throughput Screening and Automated Data-Driven Analysis of the Triplet Photophysical Properties of Structurally Diverse, Heteroleptic Iridium(III) Complexes. *J. Am. Chem. Soc.* **2021**, *143*, 1179−1194.
(31) Krass, H.; Papastavrou, G.; Kurth, D. G. Layer-by-Layer Self-Assembly of a Polyelectrolyte Bearing Metal Ion Coordination and Electrostatic Functionality. *Chem. Mater.* **2003**, *15*, 196−203.
(32) Zysman-Colman, E.; Slinker, J. D.; Parker, J. B.; Malliaras, G. G.; Bernhard, S. Improved Turn-On Times of Light-Emitting Electrochemical Cells. *Chem. Mater.* **2008**, *20*, 388−396.
(33) Li, M.-J.; Liu, X.; Shi, Y.-Q.; Xie, R.-J.; Wei, Q.-H.; Chen, G.-N. Synthesis, Structure, Photophysics and Electrochemiluminescence of Re(i) Tricarbonyl Complexes with Cationic 2,2-Bipyridyl Ligands. *Dalton Trans.* **2012**, *41*, 10612−10618.
(34) Li, M.-J.; Lin, M.; Xie, R.; Liu, X.; Wei, Q.-H.; Chen, G.-N. Synthesis and Electrochemiluminescence Studies of Tricarbonylrhenium(I) Complexes with a Cationic 2,2′-Bipyridyl Ligand. *Electrochim. Acta* **2011**, *56*, 9344−9349.
(35) Saund, S. S.; Siegler, M. A.; Thoi, V. S. Electrochemical Degradation of a Dicationic Rhenium Complex via Hoffman-Type Elimination. *Inorg. Chem.* **2021**, *60*, 13011−13020.
(36) Kerzig, C.; Guo, X.; Wenger, O. S. Unexpected Hydrated Electron Source for Preparative Visible-Light Driven Photoredox Catalysis. *J. Am. Chem. Soc.* **2019**, *141*, 2122−2127.
(37) Swords, W. B.; Li, G.; Meyer, G. J. Iodide Ion Pairing with Highly Charged Ruthenium Polypyridyl Cations in CH3CN. *Inorg. Chem.* **2015**, *54*, 4512−4519.
(38) Thordarson, P. https://Supramolecular.org (accessed Sep 14, 2021).
(39) Brynn Hibbert, D.; Thordarson, P. The Death of the Job Plot, Transparency, Open Science and Online Tools, Uncertainty Estimation Methods and Other Developments in Supramolecular Chemistry Data Analysis. *Chem. Commun.* **2016**, *52*, 12792−12805.
(40) Thordarson, P. Determining Association Constants from Titration Experiments in Supramolecular Chemistry. *Chem. Soc. Rev.* **2011**, *40*, 1305−1323.
(41) Lakowicz, J. R. *Principles of Fluorescence Spectroscopy*, 3rd ed.; Springer US: New York, 2006.
(42) Clark, C. C.; Marton, A.; Meyer, G. J. Evidence for Static Quenching of MLCT Excited States by Iodide. *Inorg. Chem.* **2005**, *44*, 3383−3385.
(43) Marton, A.; Clark, C. C.; Srinivasan, R.; Freundlich, R. E.; Narducci Sarjeant, A. A.; Meyer, G. J. Static and Dynamic Quenching of Ru(II) Polypyridyl Excited States by Iodide. *Inorg. Chem.* **2006**, *45*, 362−369.
(44) Bevernaegie, R.; Wehlin, S. A. M.; Piechota, E. J.; Abraham, M.; Philouze, C.; Meyer, G. J.; Elias, B.; Troian-Gautier, L. Improved Visible Light Absorption of Potent Iridium(III) Photo-Oxidants for Excited-State Electron Transfer Chemistry. *J. Am. Chem. Soc.* **2020**, *142*, 2732−2737.
(45) Zidan, M.; Morris, A. O.; McCallum, T.; Barriault, L. The Alkylation and Reduction of Heteroarenes with Alcohols Using Photoredox Catalyzed Hydrogen Atom Transfer via Chlorine Atom Generation. *Eur. J. Org. Chem.* **2020**, 1453−1458.
(46) Rohe, S.; Morris, A. O.; McCallum, T.; Barriault, L. Hydrogen Atom Transfer Reactions via Photoredox Catalyzed Chlorine Atom Generation. *Angew. Chem., Int. Ed.* **2018**, *57*, 15664−15669.
(47) Steinfeld, J. I.; Francisco, J. S.; Hase, W. L. *Chemical Kinetics and Dynamics*, 2nd ed.; Prentice Hall: Upper Saddle River, New Jersey, 1999.
(48) Turró, C.; Zaleski, J. M.; Karabatsos, Y. M.; Nocera, D. G. Bimolecular Electron Transfer in the Marcus Inverted Region. *J. Am. Chem. Soc.* **1996**, *118*, 6060−6067.
(49) Chiorboli, C.; Scandola, F.; Kisch, H. Quenching of Excited Tris(2,2′-Bipyridine)Ruthenium(II) by Metal 1,2-Dithiolene Complexes. *J. Phys. Chem.* **1986**, *90*, 2211−2215.
(50) Chiorboli, C.; Indelli, M. T.; Rampi Scandola, M. A.; Scandola, F. Salt Effects on Nearly Diffusion Controlled Electron-Transfer Reactions. Bimolecular Rate Constants and Cage Escape Yields in Oxidative Quenching of Tris(2,2′-Bipyridine)Ruthenium(II). *J. Phys. Chem.* **1988**, *92*, 156−163.

https://doi.org/10.1021/jacsau.2c00088
JACS Au 2022, 2, 985−995

(51) Brunschwig, B. S.; Ehrenson, S.; Sutin, N. The distance dependence of electron transfer reactions: rate maxima and rapid rates at large reactant separations. *J. Am. Chem. Soc.* **1984**, *106*, 6858−6859.
(52) Newton, M. D.; Sutin, N. Electron Transfer Reactions in Condensed Phases. *Annu. Rev. Phys. Chem.* **1984**, *35*, 437−480.
(53) Sutin, N. Theory of Electron Transfer Reactions: Insights and Hindsights. *Prog. Inorg. Chem.* **1983**, *30*, 441−498.
(54) Sutin, N. Nuclear, Electronic, and Frequency Factors in Electron-Transfer Reactions. *Acc. Chem. Res.* **1982**, *15*, 275−282.
(55) Brunschwig, B. S.; Creutz, C.; Sutin, N.; Cambridge, R.; January, U. K. Optical transitions of symmetrical mixed-valence systems in the Class II-III transition regimeElectronic supplementary information (ESI) is available: derivation of eqn. (39c), table summarizing the relationships between band maxima and band widths predicted by the two-state model and table of spectral properties of mixed-valence ruthenium(II)/(III) bridged by pyrazine and dicyanamide. See http://www.rsc.org/suppdata/cs/b0/b008034i/. *Chem. Soc. Rev.* **2002**, *31*, 168−184.
(56) Fox, L. S.; Kozik, M.; Winkler, J. R.; Gray, H. B. Gaussian Free-Energy Dependence of Electron-Transfer Rates in Iridium Complexes. *Science* **1990**, *247*, 1069−1071.
(57) Gust, D.; Moore, T. A.; Moore, A. L. Molecular Mimicry of Photosynthetic Energy and Electron Transfer. *Acc. Chem. Res.* **1993**, *26*, 198−205.
(58) Yonemoto, E. H.; Saupe, G. B.; Schmehl, R. H.; Hubig, S. M.; Riley, R. L.; Iverson, B. L.; Mallouk, T. E. Electron-Transfer Reactions of Ruthenium Trisbipyridyl-Viologen Donor-Acceptor Molecules: Comparison of the Distance Dependence of Electron-Transfer Rates in the Normal and Marcus Inverted Regions. *J. Am. Chem. Soc.* **1994**, *116*, 4786−4795.
(59) Yonemoto, E. H.; Riley, R. L.; Kim, Y. I.; Atherton, S. J.; Schmehl, R. H.; Mallouk, T. E. Photoinduced Electron Transfer in Covalently Linked Ruthenium Tris(Bipyridyl)-Viologen Molecules: Observation of Back Electron Transfer in the Marcus Inverted Region. *J. Am. Chem. Soc.* **1992**, *114*, 8081−8087.
(60) Gennett, T.; Milner, D. F.; Weaver, M. J. Role of Solvent Reorganization Dynamics in Electron-Transfer Processes. Theory-Experiment Comparisons for Electrochemical and Homogeneous Electron Exchange Involving Metallocene Redox Couples. *J. Phys. Chem.* **1985**, *89*, 2787−2794.
(61) Biner, M.; Buergi, H. B.; Ludi, A.; Roehr, C. Crystal and Molecular Structures of [Ru(Bpy)3](PF6)3 and [Ru(Bpy)3](PF6)2 at 105 K. *J. Am. Chem. Soc.* **1992**, *114*, 5197−5203.
(62) Brown, G. M.; Sutin, N. A Comparison of the Rates of Electron Exchange Reactions of Ammine Complexes of Ruthenium(II) and-(III) with the Predictions of Adiabatic, Outer-Sphere Electron Transfer Models. *J. Am. Chem. Soc.* **1979**, *101*, 883−892.
(63) Marcus, R. A. On the Frequency Factor in Electron Transfer Reactions and Its Role in the Highly Exothermic Regime. *Int. J. Chem. Kinet.* **1981**, *13*, 865−872.
(64) Wehlin, S. A. M.; Troian-Gautier, L.; Maurer, A. B.; Brennaman, M. K.; Meyer, G. J. Photophysical Characterization of New Osmium (II) Photocatalysts for Hydrohalic Acid Splitting. *J. Chem. Phys.* **2020**, *153*, 054307.
(65) Wehlin, S. A. M.; Troian-Gautier, L.; Li, G.; Meyer, G. J. Chloride Oxidation by Ruthenium Excited-States in Solution. *J. Am. Chem. Soc.* **2017**, *139*, 12903−12906.
(66) Troian-Gautier, L.; Wehlin, S. A. M.; Meyer, G. J. Photophysical Properties of Tetracationic Ruthenium Complexes and Their Ter-Ionic Assemblies with Chloride. *Inorg. Chem.* **2018**, *57*, 12232−12244.
(67) Troian-Gautier, L.; Swords, W. B.; Meyer, G. J. Iodide Photoredox and Bond Formation Chemistry. *Acc. Chem. Res.* **2019**, *52*, 170−179.
(68) Isse, A. A.; Lin, C. Y.; Coote, M. L.; Gennaro, A. Estimation of Standard Reduction Potentials of Halogen Atoms and Alkyl Halides. *J. Phys. Chem. B* **2011**, *115*, 678−684.
(69) Gorelsky, S. I.; Kotov, V. Y.; Lever, A. B. P. Vertical Ionization Energies and Electron Affinities of Ions in Solution from Outer-Sphere Charge Transfer Transition Energies. *Inorg. Chem.* **1998**, *37*, 4584−4588.
(70) Humphreys, E. K.; Allan, P. K.; Welbourn, R. J. L.; Youngs, T. G. A.; Soper, A. K.; Grey, C. P.; Clarke, S. M. A Neutron Diffraction Study of the Electrochemical Double Layer Capacitor Electrolyte Tetrapropylammonium Bromide in Acetonitrile. *J. Phys. Chem. B* **2015**, *119*, 15320−15333.
(71) Rumble, C. A.; Vauthey, E. Molecular Dynamics Simulations of Bimolecular Electron Transfer: The Distance-Dependent Electronic Coupling. *J. Phys. Chem. B* **2021**, *125*, 10527−10537.
(72) Freys, J. C.; Bernardinelli, G.; Wenger, O. S. Proton-Coupled Electron Transfer from a Luminescent Excited State. *Chem. Commun.* **2008**, *36*, 4267−4269.
(73) Morton, C. M.; Zhu, Q.; Ripberger, H.; Troian-Gautier, L.; Toa, Z. S. D.; Knowles, R. R.; Alexanian, E. J. C-H Alkylation via Multisite-Proton-Coupled Electron Transfer of an Aliphatic C-H Bond. *J. Am. Chem. Soc.* **2019**, *141*, 13253−13260.
(74) Duesing, R.; Tapolsky, G.; Meyer, T. J. Long-Range, Light-Induced Redox Separation across a Ligand Bridge. *J. Am. Chem. Soc.* **1990**, *112*, 5378−5379.
(75) Josefsson, I.; Eriksson, S. K.; Rensmo, H.; Odelius, M. Solvation Structure around Ruthenium(II) Tris(Bipyridine) in Lithium Halide Solutions. *Struct. Dyn.* **2016**, *3*, 023607.
(76) Ingold, K. U.; Lusztyk, J.; Raner, K. D. The Unusual and the Unexpected in an Old Reaction. The Photochlorination of Alkanes with Molecular Chlorine in Solution. *Acc. Chem. Res.* **1990**, *23*, 219−225.
(77) Raner, K. D.; Lusztyk, J.; Ingold, K. U. Ultraviolet/Visible Spectra of Halogen Molecule/Arene and Halogen Atom/Arene .Pi.-Molecular Complexes. *J. Phys. Chem.* **1989**, *93*, 564−570.
(78) Raner, K. D.; Lusztyk, J.; Ingold, K. U. Kinetic Analysis of Alkane Polychlorination with Molecular Chlorine. Chlorine Atom/Monochloride Geminate Pairs and the Effect of Reactive Cage Walls on the Competition between Monochloride Rotation and Chlorine Atom Escape. *J. Am. Chem. Soc.* **1988**, *110*, 3519−3524.
(79) Walling, C. The Transient Species in Radical Chlorination in Benzene Solvent. *J. Org. Chem.* **1988**, *53*, 305−308.
(80) Tsao, M.-L.; Hadad, C. M.; Platz, M. S. Computational Study of the Halogen Atom-Benzene Complexes. *J. Am. Chem. Soc.* **2003**, *125*, 8390−8399.
(81) Bühler, R. E.; Ebert, M. Transient Charge-Transfer Complexes with Chlorine Atoms by Pulse Radiolysis of Carbon Tetrachloride Solutions. *Nature* **1967**, *214*, 1220−1221.
(82) Bossy, J. M.; Buehler, R. E.; Ebert, M. Pulse Radiolysis of Organic Halogen Compounds. II. Transient Bromine-Atom Charge-Transfer Complexes Observed by Pulse Radiolysis. *J. Am. Chem. Soc.* **1970**, *92*, 1099−1101.
(83) Förgeteg, S.; Bérces, T. Laser Flash Photolysis Study of Chlorine Atom/Simple Arene π-Complexes in Carbon Tetrachloride and Acetonitrile. *J. Photochem. Photobiol., A* **1993**, *73*, 187−195.
(84) Strong, R. L.; Rand, S. J.; Britt, J. A. Charge-Transfer Spectra of Iodine Atom-Aromatic Hydrocarbon Complexes 1. *J. Am. Chem. Soc.* **1960**, *82*, 5053−5057.
(85) Benson, S. W. Some Observations on the π-Complex of Cl Atoms with Benzene. *J. Am. Chem. Soc.* **1993**, *115*, 6969−6974.
(86) McGimpsey, W. G.; Scaiano, J. C. Photochemistry of α-Chloro- and α-Bromoacetophenone. Determination of Extinction Coefficients for Halogen−Benzene Complexes. *Can. J. Chem.* **1988**, *66*, 1474−1478.
(87) Bunce, N. J.; Ingold, K. U.; Landers, J. P.; Lusztyk, J.; Scaiano, J. C. Kinetic Study of the Photochlorination of 2,3-Dimethylbutane and Other Alkanes in Solution in the Presence of Benzene. First Measurements of the Absolute Rate Constants for Hydrogen Abstraction by the "Free" Chlorine Atom and the Chlorine Atom-Benzene π-C. *J. Am. Chem. Soc.* **1985**, *107*, 5464−5472.
(88) Wasielewski, M. R.; Johnson, D. G.; Svec, W. A.; Kersey, K. M.; Minsek, D. W. Achieving High Quantum Yield Charge Separation in Porphyrin-Containing Donor-Acceptor Molecules at 10 K. *J. Am. Chem. Soc.* **1988**, *110*, 7219−7221.

https://doi.org/10.1021/jacsau.2c00088
JACS Au 2022, 2, 985−995

(89) Gaines, G. L.; O'Neil, M. P.; Svec, W. A.; Niemczyk, M. P.; Wasielewski, M. R. Photoinduced Electron Transfer in the Solid State: Rate vs Free Energy Dependence in Fixed-Distance Porphyrin-Acceptor Molecules. *J. Am. Chem. Soc.* **1991**, *113*, 719−721.

https://doi.org/10.1021/jacsau.2c00088
JACS Au 2022, 2, 985−995